Fabrication of lidocaine-loaded polymer dissolving microneedles for rapid and prolonged local anesthesia

Yanan Mao
Zhejiang Sci-Tech University
Xiufeng Zhang
Hangzhou Third People's Hospital
Yanfang Sun
Zhejiang Sci-Tech University
Zhong Shen
Hangzhou Third People's Hospital
Chao Zhong
Zhejiang Sci-Tech University
Lei Nie
Xinyang Normal University
Amin Shavandi
Université libre de Bruxelles (ULB), École polytechnique de Bruxelles
Khaydar E. Yunusov
Uzbekistan Academy of Sciences
Guohua Jiang (ghjiang_cn@zstu.edu.cn)
Zhejiang Sci-Tech University

Research Article

Keywords: microneedles, drug transdermal delivery, anesthesia, lidocaine hydrochloride

Posted Date: June 16th, 2023

DOI: https://doi.org/10.21203/rs.3.rs-3050562/v1

Abstract

There is an urgent need for research on effective interventions for pain management to improve their life quality. Traditional needle and syringe injection were used to administer the local anesthesia. However, it causes various discomforts, ranging from brief stings to trypanophobia and denial of medical operations. In this study, a dissolving microneedles (MNs) system made of composite matrix materials of polyvinylpyrrolidone (PVP), polyvinyl alcohol (PVA), and sodium hyaluronate (HA) was successfully developed for the loading of lidocaine hydrochloride (LidH). The morphology, size and mechanical properties of the MNs were also investigated. After the insertion of MNs into the skin, the matrix at the tip of the MNs was rapidly dissolved, releasing the loaded LidH to diffuse into deeper skin tissue through microchannels formed by MNs insertion. The back patching of MNs could be acted as a drug reservoir to form a prolonged local anesthesia effect due to the swelling and dissolving of MNs by absorption of interstitial fluid. The results showed that LidH MNs provided a superior analgesia up to 8 h, exhibiting a rapid and long-lasting analgesic effects. Additionally, tissue sectioning and *in vitro* cytotoxicity tests indicated that the MNs patch we developed had a favorable biosafety profile.

Introduction

Pain is a complex physiological and psychological activity which is one of the most frequent clinical symptoms.[1] Local analgesia is often achieved using anesthetic drugs to block the transmission of nerve impulses by inhibiting voltage-gated sodium channels (VGSCs), causing a blockage of sensory nerve conduction in parts of the body, and resulting in a loss of sensation.[2] Current local analgesic treatments include oral administration, commercial dressings, iontophoresis and injections, each of which has its own advantages and drawbacks. While oral administration is the most common method of administration, it undergoes first-pass metabolism in the gastrointestinal tract, which impairs the efficiency of administration and can be harmful to the gastrointestinal tract.[3] Although commercial creams and dressings are simple to apply, they exhibit slow onset, inadequate efficacy, and prolonged patient discomfort as they require drug penetration through he cutaneous stratum corneum to become effective. Iontophoresis for anesthetic drug delivery is efficient, but its equipment is expensive and complex, which may be unacceptable to most patients.[4] The subcutaneous multipoint injection is the most popular pain management method. It provides a highly effective and rapid treatment but causes pain and fear especially in children, and requires a skilled professional to administer the injection.[5] Therefore, it is of important clinical significance to develop an ideal local anesthesia system with effective, rapid onset, minimal pain, easy to load and administer with minimal user training, and without bulky equipment.[6, 7]

Recently, microneedles (MNs) have obtained considerable attention as a promising platform system for the transdermal delivery of therapeutic agents due to their advantages of minimally invasive, self-administrable, and significant reduction in pain and anxiety when inserted into the skin compared to a hypodermic needle.[8–12] Microneedles are capable of penetrating the stratum corneum and form

mechanical microchannels on the skin surface, bypassing the stratum corneum as a natural barrier to transdermal drug delivery.[13–16] Due to the special structural features of MNs, the tip of the needle could reach the dermis without touching the blood vessels and sensory nerves in the dermis after they punctured into the skin, thus realizing painless and minimally invasive transdermal drug delivery.[17, 18] Lidocaine hydrochloride (LidH) is a widely used local anesthetic drug in the clinic.[19] Considering the potential of MNs to overcome the skin barrier and reduce onset time by delivering the drug directly into the skin, the delivery of LidH by MNs has been introduced. A coated MNs was developed to deliver LidH within 4 min of onset time,[20] which greatly reduced the onset of lidocaine and increased the efficiency of anesthesia. However, the amount of coated drug was insufficient due to the limited surface area of MNs.

The focus of this study was to investigate the rapid and prolonged local anesthesia by the lidocaine hydrochloride-loaded polymer MNs (LidH MNs). The LidH-loaded MNs were fabricated using a micro-molding technique. Polyvinylpyrrolidone (PVP), polyvinyl alcohol (PVA) and sodium hyaluronate (HA) were selected as matrix of dissolving MNs due to their excellent biocompatibility and biodegradability. LidH was mixed with MNs matrix, and the back patching of MNs was worked as a drug reservoir to address low drug loading of coated MNs. The morphology, size and mechanical properties of the as-fabricated MNs were investigated as well. After the insertion of MNs into the skin, the matrix at the tip of the MNs dissolves rapidly, allowing the loaded LidH to release and diffuse into deeper skin tissue through microchannels formed by the MNs penetration into the skin. The back patching of DMNs could be acted as a drug reservoir to provide a prolonged local anesthesia effect due to the swelling and dissolving of DMNs by absorption of interstitial fluid (Fig. 1). The rapid drug release and long-term analgesic effects were tested *in vitro* and *in vivo*.

Materials and methods

All animal studies were approved by the Experimental Animal Ethics Committee of the Eyoung Pharmaceutical Research and Development Centre of Zhejiang Province and Zhejiang Sci-Tech University Laboratory Animal Ethics Committee (Number: ZJEY-20221107-05). All experiments followed the instructions of the Laboratory Animal Care and Use Guide.

2.1 Materials

Lidocaine hydrochloride (LidH, 98%), polyvinylpyrrolidone (PVP, M_w = 1,300 KDa), polyvinyl alcohol (PVA, 1788 type, alcoholysis = 87.0–89.0%), sodium chloride (NaCl), formaldehyde solution (36.0%) and rhodamine B (RhB) were purchased from Aladdin Biochemical Technology Co., Ltd (Shanghai, China). Sodium hyaluronate (HA, 95%) was obtained from McLean Biochemical Technology Co., Ltd (Shanghai, China). LidH cream (25 mg lidocaine per gram) was obtained from Tongfang Pharmaceutical Group Co. LTD (Beijing, China). Dulbecco's modified eagle medium (DMEM) culture medium was provided by ThermoFisher Scientific Co., Ltd (Shanghai, China). Pancreatin cell digestion solution, methyl thiazolyl tetrazolium (MTT), Calcein/PI cell activity and cytotoxicity test kit, and 4% paraformaldehyde fixed

solution were purchased from Shanghai Beyotime Biotechnology Co., Ltd (Shanghai, China). Dimethyl sulfoxide (DMSO,99.9%) was purchased from J&K Scientific Co., Ltd (Beijing, China). Phosphate buffer solution (PBS) was purchased from Beijing Labgic Technology Co., Ltd (Beijing, China). Mouse fibroblasts (L929) was obtained from the cell bank of the Chinese Academy of Sciences (Shanghai, China). Sprague Dawley (SD) female rats were provided by Zhejiang Eyoung Pharmaceutical Research and Development Co., Ltd (Zhejiang, China).

2.2 Preparation of MNs

The MNs patches were fabricated by a reported micro-molding technique.[21] The preparation process of LidH-loaded MNs was shown in Fig. 2A. The matrix of MNs consisted of PVP, PVA, and HA (weight ratios of PVP/PVA/HA at 1:1:1, 2:1:1, 1:2:1, and 1:1:2, respectively) was firstly prepared with a concentration of 15 wt%. The mixed solutions were stirred magnetically at 80°C for 3 h to ensure that the polymers were completely dissolved. Then, the polymer solution was sonicated to eliminate air bubbles in the solution before the MNs preparation. The polymer mixture was poured into a micro-mold (40 × 40 pyramidal needles with 800 μm needle height, 500 μm needle base, and 700 μm needle pitch) and dried at 40°C for 6 h under vacuum. The excess polymer matrix on the surface of mold was scraped off. The dried MNs were peeled from the mold, sealed and placed in a vacuum oven for subsequent use. For fabrication of LidH-loaded MNs, the same method was used except for the dissolving of a certain amount of LidH (50 wt% of polymer matrix) into the above-mentioned mixed solution. For low-dose LidH MNs, LidH MNs (I), LidH was only loaded at the tips of the MNs. For high-dose LidH MNs, LidH MNs (II), both the tips and backing patch of MNs were loaded with LidH. Each MNs was evaluated for its physical appearance and dimensions using a light microscope.

2.3 Puncture and mechanical properties test of MNs

A universal testing machine (5943, machine model, USA) was used to evaluate the mechanical properties of the MNs patch. The MNs patch was placed on a flat surface of the base plate, and the instrument parameters were set. The top stainless steel probe was moved vertically at a constant speed of 4 mm/min for a maximum test distance of 800 μm. The force-displacement curve was recorded after the top probe came into contact with the MNs patch. To test the efficiency of insertion of the MNs patch, a constant force was used to penetrate the MNs patch into fresh porcine skin. After treatment, the perforation of the porcine skin was observed by a hand-held microscope.

2.4 Stability and drug release tests of MNs

To test the MNs dissolution performance, the MNs patch was punctured into fresh porcine skin and the morphology of MNs patch was recorded at different time points to determine their dissolution performance (Fig. S1). The standard curve of LidH was firstly determined by the UV-Vis Absorption Spectrometer (UV-Vis, U3900H, Japan) method (Fig. S2). According to the LidH standard curve, the drug content of LidH MNs under different storage time for 1, 7, 14, 21 and 28 days were determined to exploit the influence of storage time on drug stability.

To determine the drug release from MNs, the as-prepared MNs patch was placed in a beaker containing 60 mL of PBS and sealed in a 37 ℃ shaker (KQ-400KDE, China). Then, 3 mL of sample was taken at set interval time and the same volume of fresh PBS was added. The LidH loading content in MNs patch was subsequently quantified using UV-Vis.

To further research the release and diffusion of drugs in the skin, an improved Franz diffusion cell was used to test drug release in vitro.[22] Firstly, the MNs patch was inserted into fresh porcine skin and then placed on a receiving chamber of the Franz diffusion cell which contained 43 mL PBS, and set a rotation speed at 600 rpm. Then, 3 mL of sample was taken from the receiving room at 0, 0.5, 1, 2, 3, 6, 12 and 24 h respectively, and the same amount of new PBS was introduced, then analyze the drug release efficiency in vitro by UV-Vis.[11, 23]

2.5 Analgesia tests *in vivo*

Female SD rats (~ 200 ± 30 g) were used in this experiment, and the animals were subjected to a 12-hour light-dark cycle at 25 ± 2°C. Food and water were fed freely during non-experimental times, and these animals were allowed to acclimatize for 2 days prior to the experiment.

The rats were randomly divided into five groups, namely blank group (healthy without treatment), blank microneedle group (without LidH), LidH MNs (I) (low dose, ~ 1 mg/patch), LidH MNs (II) (high dose, ~ 20 mg/patch) and a LidH cream group. To establish a formalin pain-induced model, the legs of rats were first dehaired. 10 minutes after the rats were administered, saline was injected subcutaneously into the right hind paw of the blank group and 5% formalin solution was injected subcutaneously into the right hind paw of the rest of experimental group, and the pain response of rats in each group was observed every 5 min for 1 h.[24]

To determine mechanical pain threshold, a 1cm wound was created by a scalpel on the right hind foot of the rats after drug administration, which was cut the epidermis by a scalpel. Von Frey fibers wires bending force at 2, 4, 6, 8, 10, 15, 26, 60 and 100 g were used to stimulate the skin of the foot under the metal cage, and each fiber wire was repeatedly stimulated 3 times.[25] If the paw was retracted 2 out of 3 times, the force was considered as its mechanical threshold. Their mechanical thresholds were measured before and after wound scratching at 0, 0.5, 1, 2, 4 and 8 h, respectively.

2.6 Biocompatibility

The cytocompatibility of LidH-loaded MNs was determined by MTT method. Briefly, L929 cells were cultured in a 96-well plate at a density of 1×10^5 cells, which were incubate for 24 h. And then, 10 μL of the MNs leaching solutions with 0, 25, 50, 100 and 200 μg/mL were added into per well. After cells and material were co-cultured for 12 h, 20 μL MTT was added into each well and stained for 4h protected from light. Subsequently, 150 μL DMSO was added to each well and its absorbance was measured at 490 nm using an enzyme marker (LM-MK3, American). To assess the inflammatory effects *in vivo*, the MNs patch were applied to the dorsal skin of rats for 6 h, followed by hematoxylin-eosin (H&E) staining and

toluidine blue (TB) staining. The weight of animals, food and water consumption were monitored daily during the experiment process.

2.7 Statistical analysis

All samples that need to be analyzed are carried out with a sample size of $n \geq 3$, and Excel, Origin and GraphPad are used for statistical analysis. Data describing statistics were expressed as mean ± standard deviation. One-way ANOVA was used for comparisons between data points. Differences were considered to be statistically significant when $P \leq 0.05$ (*$P < 0.05$, **$P < 0.01$, ***$P < 0.001$).

Results and discussion

3.1 Characterization of MNs

Pyramidal-shaped MNs comprised of PVP, PVA and HA were fabricated via the simple and affordable casting of aqueous solutions polymer matrix using female master molds (Fig. 2A). These polymers were chosen for their high water solubility and biocompatibility, enabling the formulation of dissolvable MNs to deliver therapeutic drugs through the skin.[26–30] Each microneedle patch consists of a needle tip and a drug-loaded backing patch. Figure 2B shows the morphology of LidH-loaded MNs. The resulting MNs array consists of 40 x 40 arrays, each needle with a base diameter of 440 μm, and a needle tip distance of 700 μm and a height of 760 μm (Fig. 2BI-III). The length of the MNs far exceeds the thickness of the human stratum corneum (50–100 μm).[31] Thus, the MNs can only penetrate the stratum corneum of the skin to reach the epidermis and will not reach the blood vessels in the dermis and the sensory nerves, causing no bleeding or pain.[32] In addition, the MNs surface is smooth and free of particles, indicating the excellent dispersibility of the drug in polymer matrix.[33] As shown in Fig. 2B, the MNs patch can be bant in all direction, indicating its good flexibility, thus allowing for a better fit to the skin during application and reducing the likelihood of detachment.

In order to verify whether the MNs patch has sufficient mechanical strength to penetrate the skin stratum corneum, the mechanical properties of the MNs patch were tested using a universal testing machine. As shown in Fig. 2C, an axial compressive load is applied to the MNs patch and the force-displacement curves are recorded against the compressive displacement. Previous reports[34] demonstrated that MNs with a hardness of 0.045 N/needle could penetrate the stratum corneum. The mechanical hardness values of all MNs are > 0.1 N/needle and greater when compressed to a displacement of 400 μm. These results indicate that the as-fabricated MNs have sufficient stratum corneum piercing performance. The mechanical hardness values with different composition ratios show a slight difference. The MNs with PVP : PVA : HA at 1 : 2 : 1 and 2 : 1 : 1 shows the better mechanical hardness values than that at 1 : 1 : 1 and 1 : 1 : 2. In addition, due to the best toughness and flexibility of polymer matrix with composition ratios of PVP, PVA, and HA at 1 : 2 : 1, this composition ratio was selected to fabricate MNs to provide sufficient mechanical support as well as flexibility for the following study.

To further verify the skin penetration ability of MNs patch, skin puncture experiments were performed using blank MNs patch and RhB-loaded MNs, respectively. Fresh porcine skin was selected, the fat was scraped off using a scalpel, the MNs patch was applied to the skin and pressed using the thumb for 1 min. As shown in Fig. 2D, after the removal of the MNs patch, a regular array of micropores were left on the surface of the porcine skin, indicating that the MNs patch can successfully penetrate the skin. RhB, a model drug, was used to assist in observing the penetration performance of MNs for porcine skin. As anticipated, the RhB-loaded MNs penetrated the porcine skin with all of the needles in the MN array, resulting in the visible release of dye into the skin. Furthermore, no excess material remained on the porcine skin after administration which brought higher biological safety. In addition, the hematoxylin-eosin (H&E) stained histological section image shows that as-fabricated MNs is able of penetrating the skin with the depth of ~ 300 μm (Fig. 2E). The microchannel can be also observed in Fig. 2F, which indicates that as-fabricated MNs can effectively penetrate the skin.

3.2 Stability and drug release of LidH-loaded MNs

The LidH standard curve was first determined by UV-Vis (Fig. S2). Then, the as-fabricated LidH-loaded MNs were further soaked in PBS to determine the content of LidH in the soaking solution, which was 7.59 ± 0.099 and 157.78 ± 0.163 mg/patch for LidH MNs and LidH MNs I, as calculated by fitting with the standard curve (Table S1). Using backing patch as a drug reservoir can significantly enhance the drug loading capacity of the MNs patch.

The storage stability of MNs patches is also tested against storage time. As shown in Fig. 3A and B, the relationship between the stability of MNs and the storage time has been determined. The results indicate that the stability of MNs remained constant over a storage period of 4 weeks, as evidenced by the negligible difference in weight among the tested group. Additionally, the drug loading of each group exceeds 97%, indicating that the stability of LidH in MNs was not significantly affected by storage time. This may be due to the resistance of matrix of MNs to external impurities, thus protecting the LidH from degradation.

A prominent advantage involved in the proposed MNs patch is that it facilities continuous transdermal delivery of LidH, thereby improving the efficiency of local and long-lasting analgesia. Thus, the drug delivery profiles of the as-fabricated MNs patches were evaluated by using *in vitro* PBS drug release and rat skin-based drug release tests. Figure 3C and Fig. S3 shows the LidH release against soaking time. More than 90% LidH can be released within 1 h due to the excellent dissolving properties of matrix of MNs (LidH MNs). To simulate the drug delivery *in vivo*, a modified Franz diffusion cell was used to measure drug delivery efficiency. The MNs patch was inserted into fresh porcine skin using a thumb, and the treated skin was then placed over a receiving chamber containing PBS solution. 3 mL of the sample was taken at fixed time intervals from the receiving chamber, following the addition of an equal amount of PBS to the chamber. The drug release content was calculated by a standard drug curve. As shown in Fig. 3D, the LidH MNs shows a rapid release within 2 h (~ 60%) due to the rapid dissolving of MNs in the skin tissue. After that, the amount of drug release can be further increased with ~ 95% after 12 h. However, in the case of LidH cream, only ~ 50% delivery efficiency can be obtained after 12 h. It indicates

that drug delivery efficiency can be improved through microchannels formed by MNs. In the case of LidH MNs , a rapid release within 2 h (~ 55%) also can be observed, and cumulative release of LidH can be enhanced to 70.94% after 12 h. The relatively lower cumulative release of LidH MNs may be contributed to the inability of the drug in the backing patch to fully penetrate the skin through microchannels.

3.3 Analgesia tests *in vivo*

To evaluation the analgesic effect of LidH MNs, a formalin-induced pain model was established (Fig. 4A and Fig. S4C). The licking and twisting time of rats were recorded every 5 min for 1 h. The blank control group (without any treatment) had a slight reaction after injection of saline, less than 15 s within 1 h, as shown in Fig. 4B. Following formalin injection, the blank MNs group (without drug treatment), exhibited acute pain as evidenced by a licking time lasting 92 s within first 5 min, followed by a decrease into a “quiet period” to < 5 s of the licking time at 5–15 min. After that, it increased to ~ 62 s again after 20 min, and decreased slowly to a normal state after 1 h. This is consistent with the previous report that there is an acute pain response lasting about 5 min (phase I), followed by a quiet period of about 10 min, and then a pain response that lasts for 40–50 minutes (phase II).[35–37] Compared with LidH cream group, a two-phase pain response phenomenon still be observed in the LidH MN (I) and LidH MN (II) groups. Furthermore, no significant differences were found among all tested groups within 5 min (Fig. 4B), implying no drug effect formed in such a short time because the drug has not sufficiently diffused and absorbed into nerve endings. However, in the phase II pain stage, the licking time for LidH-loaded MNs was significantly lower than that of the blank control and LidH cream group. In addition, the licking time for high-dose LidH-loaded MNs (~ 30 s after formalin injection for 25 min) was lower than that of low-dose LidH-loaded MNs (~ 38 s after formalin injection for 25 min). Besides, no significant difference in licking time can be found between the LidH cream group and blank MNs group during the first 30 min, while there is more significant difference in licking time between LidH MNs groups and blank MNs group, suggesting that as-fabricated MNs has a faster onset of action than that of LidH cream. There is no significant difference in phase I between the blank MNs, LidH MNs and LidH cream groups (Fig. 4C). And in the phase II, the twist licking number of LidH MNs treatment group is significantly shorter than that of blank MNs group. Specifically, compared to the blank MNs group, the twisting number in the LidH-loaded MNs (I) group is reduced by 50% of the blank group, and only 25% for the LidH-loaded MNs (II) group, indicating the better analgesic effect of as-fabricated high-dose LidH-loaded MNs. In addition, compared with the LidH cream group, the LidH-loaded MNs group has a better inhibitive effect on painful reactions. This may be due to the fact that MNs can pierce the stratum corneum of the skin, improving drug diffusion and absorption. LidH can block VGSCs, decrease cell membrane permeability to Na^+, prevent cell membrane depolarization and reversibly block axonal nerve impulse generation and conduction, resulting in loss of sensation, and achieving efficient and rapid analgesia.[38] These results indicate that LidH can be efficiently delivered into nerve endings via the transdermal delivery route.

A mechanical pain threshold test was designed to evaluate the long-lasting analgesia of our designed MNs patches. After 10 minutes of administration, all the test animals were scratched on the right hind foot with a sterile scalpel. Their mechanical pain threshold was tested by Von Frey filament before and

after the ws wound created (Fig. S4D). According to the previous report,[39] the nociceptive receptors of animal tend to become more sensitive following tissue injure, resulting in a lowered heat or mechanical threshold. In this study, the pre-surgical mechanical thresholds of the rats in each experimental group were established as a reference (100%). Following a hind foot scratch, the nociception became more sensitive, leading to a reduction in mechanical thresholds by approximately 14%. As shown in Fig. 4D, no significant changes were observed in the blank control and blank MNs groups. However, the mechanical threshold of rats treated by LidH MNs (II) increases rapidly to 86% within 2 h, then decrease but remain above 37% even after 8 h. In addition, the mechanical thresholds of LidH-loaded MNs groups are higher than that of LidH cream and bank groups. Besides, there is no significant difference in the LidH MNs group and blank MNs group in the first 30 min, while there is significantly improve of mechanical pain threshold in the LidH loaded MNs group (inset of Fig. 4D). These results indicate that as-fabricated MNs is able of achieving not only long- lasting analgesia, but also rapid onset. Figure 4E shows the integral area of mechanical threshold change for all test groups from 0 to 8 h after administration. The integral area of mechanical threshold for the LidH MNs (I) and LidH MNs (II) groups are 2.5 and 3.5 times greater than that of LidH cream group, respectively (Fig. 4E), indicating the superior analgesic effect of MNs. The high-dose LidH-loaded MNs groups show the highest integral area of mechanical threshold change, indicating the best long-lasting analgesia effect.

Possible longer-term effects of LidH-loaded MNs to the anaesthetic management were determined by measuring growth and dietary. Daily food and water consumption are calculated for each rat taking into account the experimental periods in comparison with health group. As shown in Fig. 4F and G, except for the animals exposed to blank MNs group, the daily food and water consumption in LidH-loaded MNs are similar in blank health group. Among them, the daily food and water consumption in high-dose LidH-loaded MNs are closer to the health state, indicating a better pain relief effect. In addition, mean weight changes of rats exhibit a similar trend compared with daily food and water consumption (Fig. 4H). These results imply that MNs can effectively produce a longer-term analgesic effect through the transdermal delivery of analgesics.

3.4 Biocompatibility

To further assess the safety of the matrix and as-fabricated MNs, an MTT method has been used to evaluate cytotoxic activity by co-culture of them with L929 cells for 24 h. Based on Fig. 5A, the cell viability of MNs matrix and LidH-loaded MNs remained at more than 85% even when the concentration of the MNs matrix was increased to 200 μg/mL, except for the true LidH. This suggests that the MNs matrix and LidH-loaded MNs are non-cytotoxic.[40] There is no significant difference between blank MNs and LidH-loaded MNs (with LidH at 50 μg/mL) (Fig. 5B). To further assess the cytotoxicity of the matrix of MNs and LidH-loaded MNs, the Calcein/PI cell activity was evaluated on the cell proliferation by co-culture of matrix with L929 cells for 24 and 48 h. As shown in Fig. 5C, the spindle-shaped characteristic can be clearly observed in all group, and the number of cells can be significantly enhanced with increasing the co-culture time. However, the number of cells in high-dose LidH-loaded MNs is slightly less

than the low-dose LidH-loaded and blank MNs after co-culture for 48 h. In addition, no dead cells can be observed in all groups, indicating that the as-fabricated MNs patch possesses excellent biocompatibility.

Histological analysis was used to further evaluate the inflammatory effects after MNs treatment. No significant inflammatory reaction and thickening of the epithelium can be observed after MNs treatment. The toluidine blue-stained can be used for staining collagen tissue, which can indicate the density of newly formed collagen by the depth of the colour. As shown in Fig. 5D and Fig. S5, there is more new collagen formations in blank and low-dose LidH-loaded MNs than the high-dose LidH-loaded MNs group, especially in the superficial areas of skin. In addition, there is a regular arrangement of collagen in the control, blank and LidH MNs (I) groups, showing a dense packing and parallel manner with the collagen-fibrils. This structure of collagen can also observe in the LidH MNs (II) group, but less than that of control group. These results indicate that the high-dose MNs group is relatively unfavorable for cell proliferation, but still has a good biological safety. In addition, there is no significant difference in the number of mass cells between control group and experience group (blank MNs group, LidH MNs (I) and LidH MNs (II)), which is confirmed by toluidine blue staining, further indicating the biological safety of as-fabricated MNs.

Conclusion

In summary, we designed a LidH MNs with a rapidly dissolvable needle tip that upon application of the MNs patch to the skin, rapidly dissolves and releases the drug loaded therein, while creating mechanical micro-pore channels on the skin surface, to achieve continuous drug release from the substrate, with increased drug loading and long-lasting release of lidocaine, resulting in long-lasting analgesia. Our MNs patch had a fast drug onset time and high drug delivery efficiency. To evaluate the analgesic effect of LidH MNs, we utilized a formalin analgesia model and also performed mechanical pain tests. Our results showed that LidH MNs provided superior analgesia up to 8 h. Additionally, tissue sectioning and *in vitro* cytotoxicity tests indicated that the MNs patch we developed had a favorable biosafety profile. This study provided a convenient and safe new approach to achieving local long-lasting analgesia using MNs.

Declarations

Data availability statement

The data cannot be made publicly available upon publication because no suitable repository exists for hosting data in this field of study. The data that support the findings of this study are available upon reasonable request from the author.

Acknowledgements

This work was supported by the Huadong Medicine Joint Funds of the Zhejiang Provincial Natural Science Foundation of China (LHDMZ23H300003), National Natural Science Foundation of China (51873194), and Science and Technology Project of Hangzhou Health Commission (20220919Y011), the

General Program Foundation from the Science and Technology Bureau of Hangzhou City (20171226Y17), and the General Program Foundation from the Hangzhou City Health Bureau (A20210250).

Conflict of interest

There are no conflicts of interest.

References

1. Pain S. Painful progress. Nature 2016, 535(7611): 518-519.
2. Goodwin G, Mcmahon S B. The physiological function of different voltage-gated sodium channels in pain. Nature Reviews: Neuroscience, 2021, 22(5): 263-274.
3. Zhao Z Q, Chen B Z, Zhang X P, Zheng H, Guo X D. An update on the routes for the delivery of donepezil. Molecular Pharmaceutics, 2021, 18(7): 2482-2494.
4. Viscusi E R, Reynolds L, Tait S, Melson T, Atkinson L E. An iontophoretic fentanyl patient-activated analgesic delivery system for postoperative pain: a double-blind, placebo-controlled trial. Anesthesia and Analgesia, 2006, 102(1): 188-194.
5. Baek S H, Shin J H, Kim Y C. Drug-coated microneedles for rapid and painless local anesthesia. Biomedical Microdevices, 2017, 19(1): 2.
6. Zhan H H, Ma F S, Huang Y C, Zhang J, Jiang X Y, Qian Y C. Application of composite dissolving microneedles with high drug loading ratio for rapid local anesthesia. European Journal of Pharmaceutical Sciences, 2018, 121: 330-337.
7. Feng M J, Jiang G H, Sun Y F, Aharodnikau U E, Yunusov K E, Liu T Q, Zeng Z Y, Solomevich S O. Integration of metformin-loaded mesoporous bioactive glass nanoparticles and free metformin into polymer microneedles for transdermal delivery on diabetic rats. Inorganic Chemistry Communications, 2022, 144: 109896.
8. Wang R, Wang H, Jiang G, Sun Y, Liu T, Nie L, Shavandi A, Yunusov K E, Aharodnikau U E, Solomevich S O. Transdermal delivery of allopurinol to acute hyperuricemic mice via polymer microneedles for the regulation of serum uric acid levels. Biomater Sci, 2023, 11(5): 1704-1713.
9. Khan S, Hasan A, Attar F, Babadaei M M N, Zeinabad H A, Salehi M, Alizadeh M, Hassan M, Derakhshankhah H, Hamblin M R, Bai Q, Sharifi M, Falahati M, Ten Hagen T L M. Diagnostic and drug release systems based on microneedle arrays in breast cancer therapy. Journal of Controlled Release, 2021, 338: 341-357.
10. Song G, Jiang G H, Liu T Q, Zhang X Y, Zeng Z Y, Wang R F, Li P F, Yang Y H. Separable Microneedles for Synergistic Chemo-Photothermal Therapy against Superficial Skin Tumors. ACS Biomaterials Science & Engineering, 2020, 6(7): 4116-4125.
11. Ruan L M, Song G, Zhang X Y, Liu T Q, Sun Y F, Zhu J L, Zeng Z Y, Jiang G H. Transdermal delivery of multifunctional CaO2@Mn-PDA nanoformulations by microneedles for NIR-induced synergistic

therapy against skin melanoma [J]. Biomaterials Science, 2021, 9(20): 6830-6841.

12. Liu T, Sun Y, Jiang G, Zhang W, Wang R, Nie L, Shavandi A, Yunusov K E, Aharodnikau U E, Solomevich S O. Porcupine-inspired microneedles coupled with an adhesive back patching as dressing for accelerating diabetic wound healing. Acta Biomaterialia, 2023, 160: 32-34.
13. Caffarel-Salvador E, Kim S, Soares V, Tian R Y, Stern S R, Minahan D, Yona R, Lu X Y, Zakaria F R, Collins J, Wainer J, Wong J, Mcmanus R, Tamang S, Mcdonnell S, Ishida K, Hayward A, Liu X W, Hubalek F, Fels J, Vegge A, Frederiksen M R, Rahbek U, Yoshitake T, Fujimoto J, Roxhed N, Langer R, Traverso G. A microneedle platform for buccal macromolecule delivery. Science Advances, 2021, 7(4): 11.
14. Amani H, Shahbazi M A, D'amico C, Fontana F, Abbaszadeh S, Santos H A. Microneedles for painless transdermal immunotherapeutic applications. J Controlled Release, 2021, 330: 185-217.
15. Wang R, Jiang G H, Aharodnikau U E, Yunusov K, Sun Y F, Liu T Q, Solomevich S O. Recent advances in polymer microneedles for drug transdermal delivery: design strategies and applications. Macromolecular Rapid Communications, 2022, 43(8): 2200037.
16. Liu T Q, Jiang G H, Song G, Zhu J Y, Yang Y H. Fabrication of separable microneedles with phase change coating for NIR-triggered transdermal delivery of metformin on diabetic rats. Biomedical Microdevices, 2020, 22(1): 12.
17. Li X J, Shan W T, Yang Y, Joralmon D, Zhu Y Z, Chen Y Y, Yuan Y, Xu H, Rong J H, Dai R, Nian Q, Chai Y, Chen Y. Limpet tooth-inspired painless microneedles fabricated by magnetic field-assisted 3D printing. Advanced Functional Materials, 2021, 31(5): 11.
18. Seeni R Z, Zheng M, Lio D C S, Wiraja C, Mohd Yusoff M F B, Koh W T Y, Liu Y, Goh B T, Xu C. Targeted Delivery of Anesthetic agents to bone tissues using conductive microneedles enhanced iontophoresis for painless dental anesthesia. Advanced Functional Materials, 2021, 31(47): 2105686.
19. Voute M, Morel V, Pickering G. Topical lidocaine for chronic pain treatment. Drug Design Development and Therapy, 2021, 15: 4091-4103.
20. Wang Q L, Zhu D D, Chen Y, Guo X D. A fabrication method of microneedle molds with controlled microstructures. Materials Science & Engineering C-Materials for Biological Applications, 2016, 65: 135-142.
21. Song G, Sun Y F, Liu T Q, Zhang X Y, Zeng Z Y, Wang R F, Li P F, Li C H, Jiang G H. Transdermal delivery of Cu-doped polydopamine using microneedles for photothermal and chemodynamic synergistic therapy against skin melanoma. Chemical Engineering Journal, 2021, 426: 10.
22. Liu Y, Cheng M, Zhao J, Zhang X, Huang Z, Zang Y, Ding Y, Zhang J, Ding Z. Transdermal delivery of lidocaine-loaded elastic nano-liposomes with microneedle array pretreatment. Biomedicines, 2021, 9(6): 592.
23. Zhang X Y, Jiang G H, Song G, Liu T Q, Sun Y F, Zeng Z Y. Fabrication of h-MnO_2@PDA composite nanocarriers for enhancement of anticancer cell performance by photo-chemical synergetic therapies. Frontiers of Materials Science, 2021, 15(2): 291-298.

24. Mcnamara C R, Mandel-Brehm J, Bautista D M, Siemens J, Deranian K L, Zhao M, Hayward N J, Chong J A, Julius D, Moran M M, Fanger C M. TRPA1 mediates formalin-induced pain. Proceedings of the National Academy of Sciences of the United States of America, 2007, 104(33): 13525-13530.
25. Chaplan S R, Bach F W, Pogrel J W, Chung J M, Yaksh T L. Quantitative assessment of tactile allodynia in the rat paw. Journal of Neuroscience Methods, 1994, 53(1): 55-63.
26. Liu D P, Yu B, Jiang G H, Yu W J, Zhang Y, Xu B. Fabrication of composite microneedles integrated with insulin-loaded $CaCO_3$ microparticles and PVP for transdermal delivery in diabetic rats. Materials Science & Engineering C-Materials for Biological Applications, 2018, 90: 180-188.
27. Abdelghany S, Tekko I A, Vora L, Larraneta E, Permana A D, Donnelly R F.
28. Jang D, Tang J, Schwendeman S P, Prausnitz M R. Effect of surface interactions on microsphere loading in dissolving microneedle patches. ACS Appl Mater Interfaces, 2022, 14(26): 29577-29587.
29. Ray S, Wirth D M, Ortega-Rivera O A, Steinmetz N F, Pokorski J K. Dissolving microneedle delivery of a prophylactic HPV vaccine. Biomacromolecules, 2022, 23(3): 903-912.
30. Yang Y, Chu H, Zhang Y, Xu L, Luo R, Zheng H, Yin T, Li Z. Rapidly separable bubble microneedle patch for effective local anesthesia. Nano Research, 2022, 15(9): 8336-8344.
31. Kim J Y, Han M R, Kim Y H, Shin S W, Nam S Y, Park J H. Tip-loaded dissolving microneedles for transdermal delivery of donepezil hydrochloride for treatment of Alzheimer's disease [J]. European Journal of Pharmaceutics and Biopharmaceutics, 2016, 105: 148-155.
32. Ma G, Wu C. Microneedle, bio-microneedle and bio-inspired microneedle: A review [J]. Journal of Controlled Release, 2017, 251: 11-23.
33. Tassanapukdee Y, Prayongpan P, Songsrirote K. Removal of heavy metal ions from an aqueous solution by CS/PVA/PVP composite hydrogel synthesized using microwaved-assisted irradiation [J]. Environmental Technology & Innovation, 2021, 24: 14.
34. Gao B B, Guo M Z, Lyu K, Chu T S, He B F. Intelligent Silk Fibroin Based Microneedle Dressing (i-SMD). Advanced Functional Materials, 2021, 31(3): 2006839.
35. Gwon D H, Kim S I, Lee S H, Noh C, Kim Y, Yun S, Lee W H, Oh J Y, Kim D W, Hong J, Lee S Y. NFAT5 Deficiency Alleviates Formalin-Induced Inflammatory Pain Through mTOR [J]. International Journal of Molecular Sciences, 2021, 22(5): 2587.
36. Mckenna J E, Melzack R. Dissociable effects of lidocaine injection into medial versus lateral thalamus in tail-flick and formalin pain tests [J]. Pathophysiology, 1994, 1(3): 205-214.
37. Yang C-L, Jing J-J, Fu S-Y, Zhong Y-L, Su X-Z, Shi Z-M, Wu X-Z, Yang F, Chen G-Z. Ropivacaine-induced seizures evoked pain sensitization in rats: Participation of 5-HT/5-HT3R [J]. Neurotoxicology, 2022, 93: 173-185.
38. Hermanns H, Hollmann M W, Stevens M F, Lirk P, Brandenburger T, Piegeler T, Werdehausen R. Molecular mechanisms of action of systemic lidocaine in acute and chronic pain: a narrative review [J]. British Journal of Anaesthesia, 2019, 123(3): 335-349.

39. Basbaum A I, Bautista D M, Scherrer G, Julius D. Cellular and Molecular Mechanisms of Pain [J]. Cell, 2009, 139(2): 267-284.
40. Van De Loosdrecht A A, Nennie E, Ossenkoppele G J, Beelen R H, Langenhuijsen M M. Cell mediated cytotoxicity against U 937 cells by human monocytes and macrophages in a modified colorimetric MTT assay. A methodological study [J]. Journal of Immunological Methods, 1991, 141(1): 15-22.

Figures

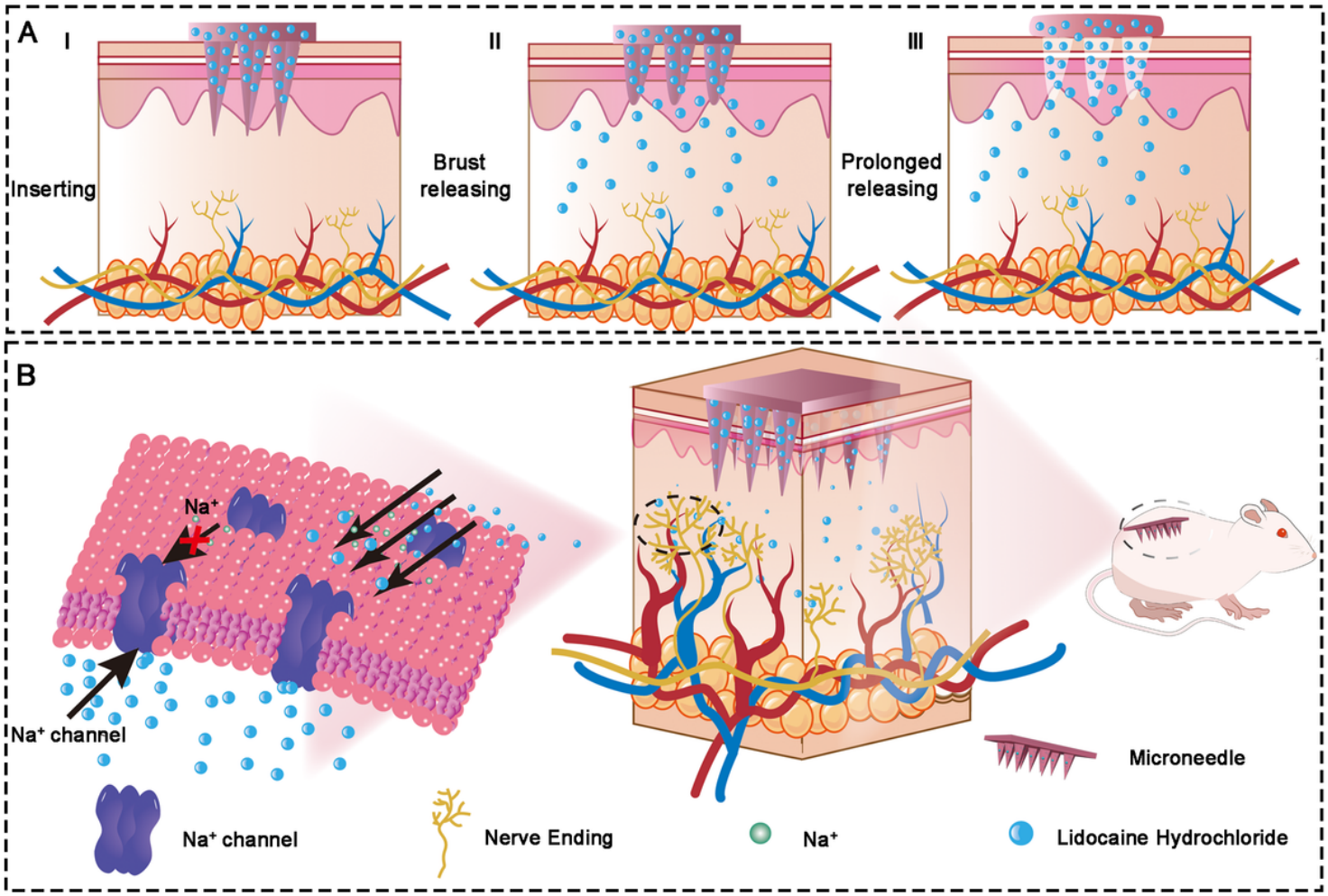

Figure 1

(A) Diagram of MNs application and the LidH MNs for drug delivery, and (B) Diagram of MNs patch application in SD rat and the mechanism of lidocaine's action.

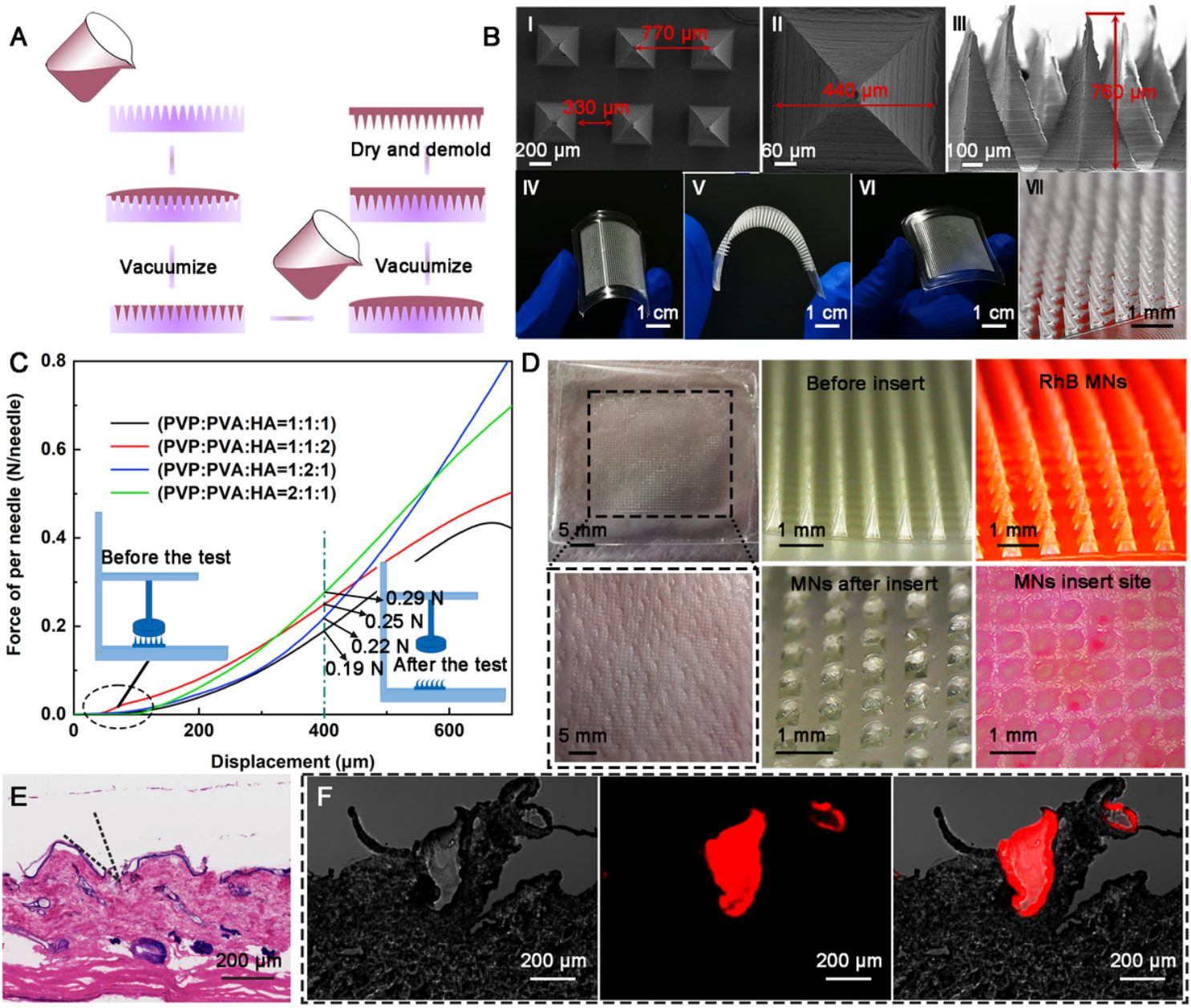

Figure 2

(A) Schematic diagram of the ffabrication process of MNs, (B) morphology of LidH MNs image by SEM and optical microscopy, (C) characterization of the mechanical property of LidH MNs, and (D) insertion proportion of MNs for skin and Morphology of MN before and after treatment, (E) H&E-stained histological section image of rat skin after the removal of MN *vitro,* (F) fluorescent images of histological sections after insertion by RhB MNs.

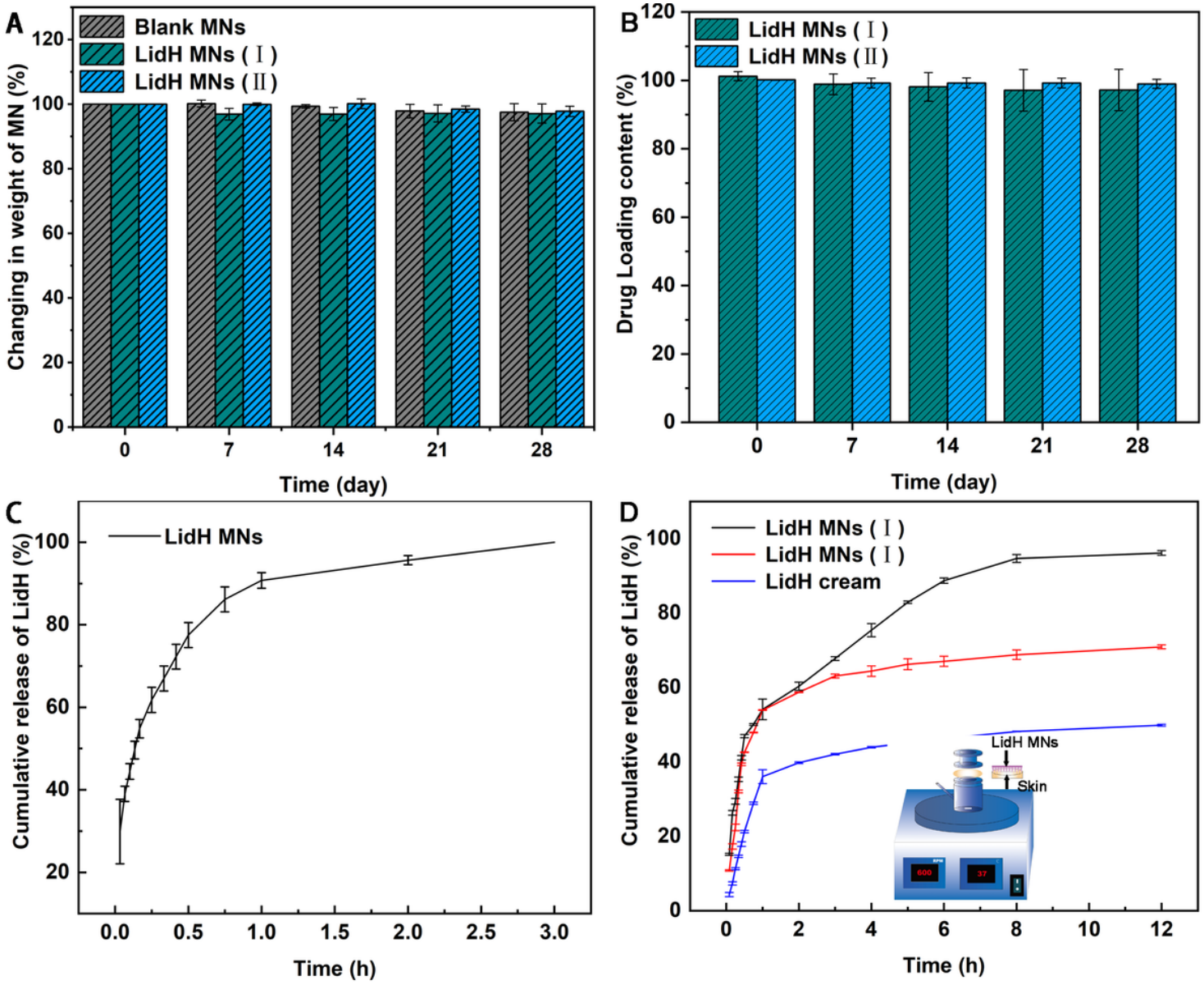

Figure 3

(A) The mass changes of LidH-loaded MNs at different storage times, (B) drug stability of LidH-loaded MNs under various storage times, (C) *in vitro* drug release curve in PBS solution, and (D) *in vitro* skin drug release profiles of LidH-loaded MNs.

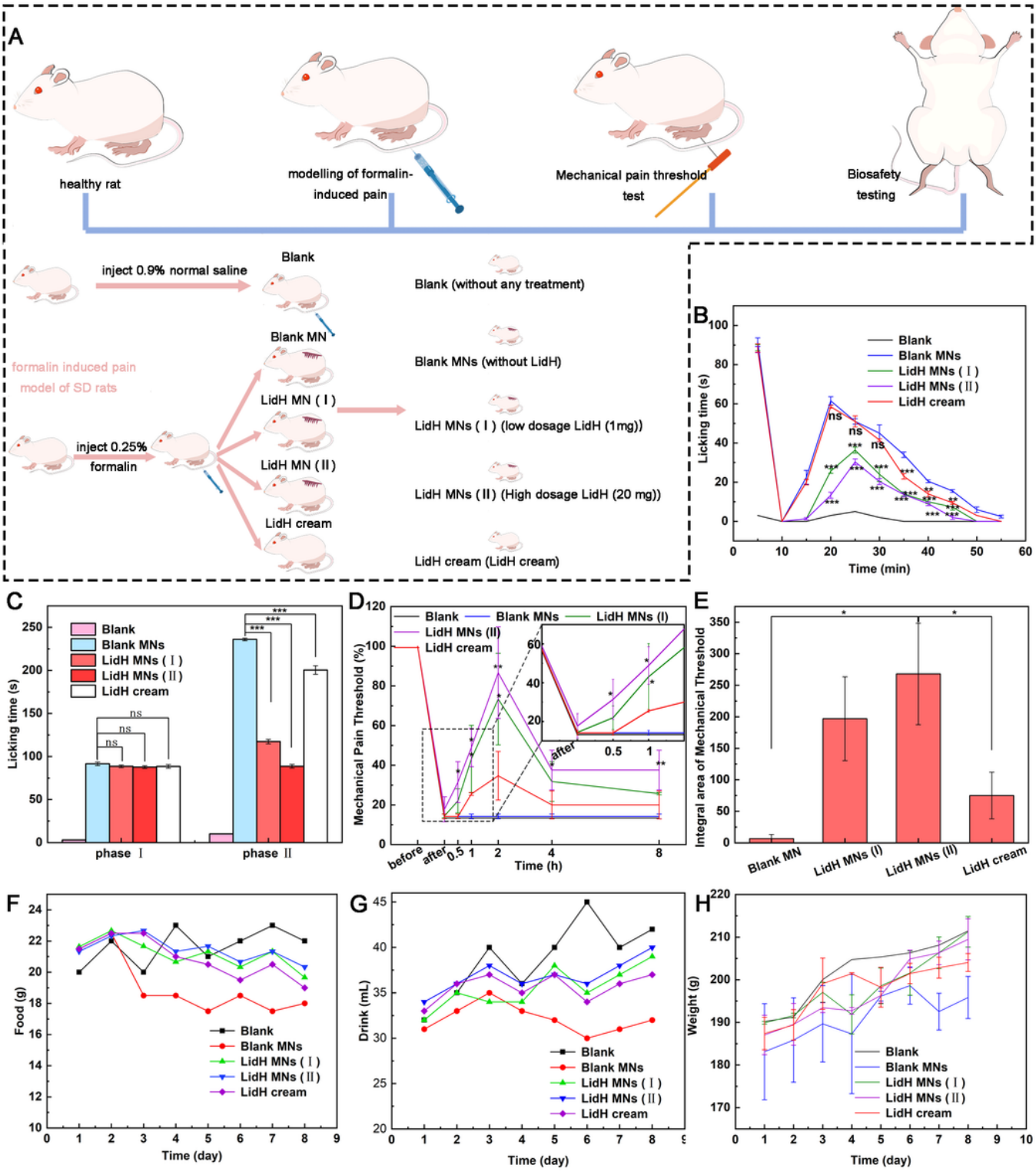

Figure 4

(A) Treatment strategy of LidH-loaded MNs for analgesia on the pain SD rats and modelling of formalin-induced pain on SD rats, (B) licking time of SD rats every 5 minutes for one hour of Formalin induced pain model, (*P<0.05, **P<0.01, ***P<0.001 for LidH-loaded MNs/LidH cream *vs.* Blank MNs), (C) licking time of formalin induced pain of SD rats in the phase (I) and (II) stages, (*P<0.05, **P<0.01, ***P<0.001 for LidH-loaded MNs/LidH cream *vs.* blank MNs), (D) mechanical pain threshold in injure SD rats,

(*P<0.05, **P<0.01, ***P<0.001 for LidH-loaded MNs/LidH cream *vs.* blank MNs), (E) area of integration under the mechanical pain threshold curve, (*P<0.05, **P<0.01, ***P<0.001 for blank MNs/LidH cream *vs.* LidH-loaded MNs), (F) food and water consumption (G) and (H) weight changes of SD rats during the experiment process.

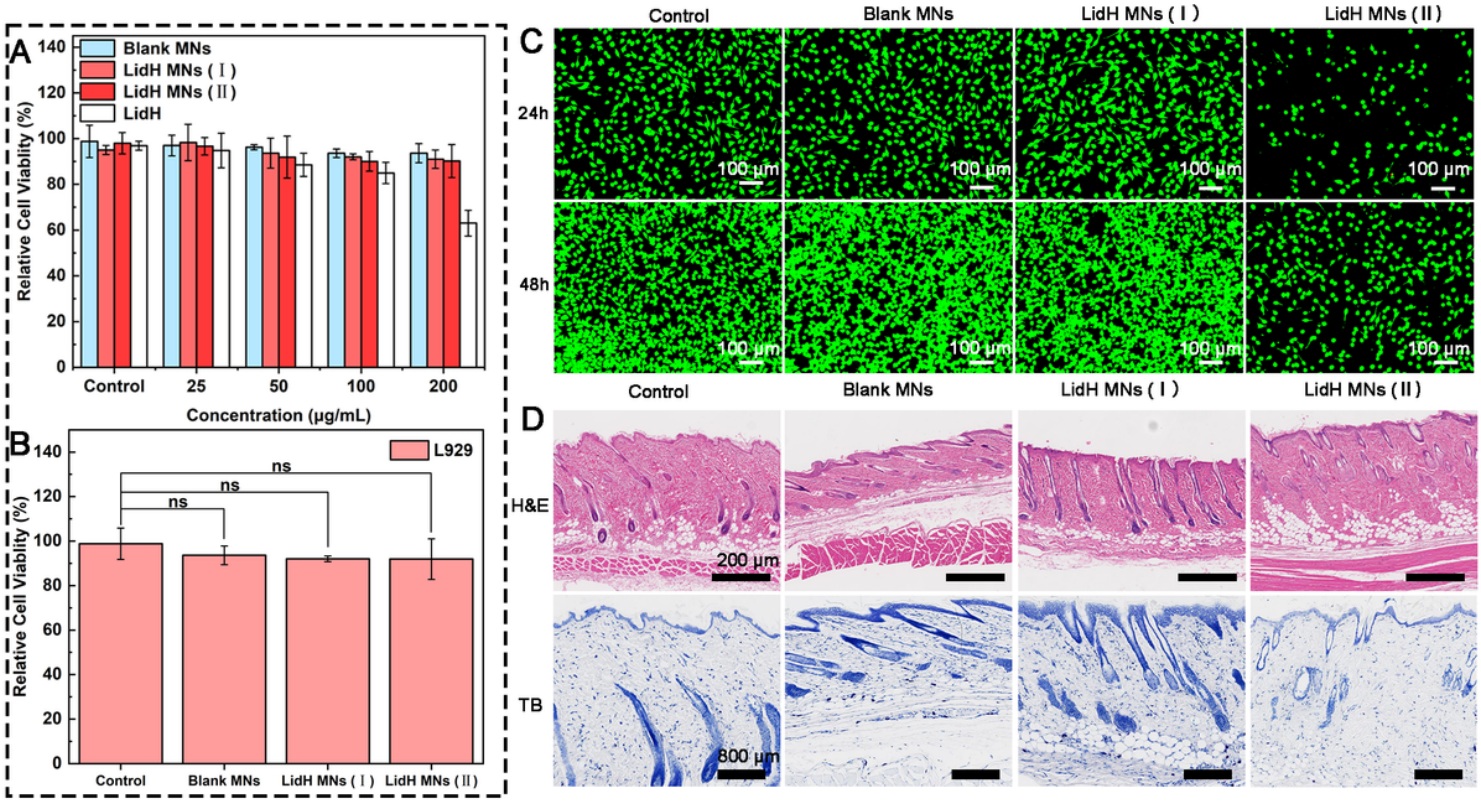

Figure 5

(A) and (B) Relative cell viability of L929 incubated with extracts of different concentrations of LidH MNs after 24h, (Blank MNs/LidH-loaded MNs ( )/LidHloaded MNs ( ) *vs* control), (C) fluorescently imaged of L929 cells incubated with extracts of different kind of the extracts of MNs after 24 and 48 h, (D) hematoxylin-eosin (H&E) and toluidine blue (TB)staining images of skin tissue.

Supplementary Files

This is a list of supplementary files associated with this preprint. Click to download.

- ElectronicSupplementaryInformation.doc